Light-Scattering Detection Hot Paper

International Edition: DOI: 10.1002/anie.201603007
German Edition: DOI: 10.1002/ange.201603007

Label-Free Analysis of Single Viruses with a Resolution Comparable to That of Electron Microscopy and the Throughput of Flow Cytometry

*Ling Ma[+], Shaobin Zhu[+], Ye Tian, Wenqiang Zhang, Shuo Wang, Chaoxiang Chen, Lina Wu, and Xiaomei Yan**

Abstract: *Viruses are by far the most abundant biological entities on our planet, yet existing characterization methods are limited by either their speed or lack of resolution. By applying a laboratory-built high-sensitivity flow cytometer (HSFCM) to precisely quantify the extremely weak elastically scattered light from single viral particles, we herein report the label-free analysis of viruses with a resolution comparable to that of electron microscopy and the throughput of flow cytometry. The detection of single viruses with diameters down to 27 nm is described. T7 and lambda bacteriophages, which differ in size by as little as 4 nm, could be baseline-resolved. Moreover, subtle structural differences of the same viral particles can be discriminated. Using monodisperse silica nanoparticles as the size reference standards, the virus sizes measured by the HSFCM are in agreement with the equivalent particle diameters derived from their structural dimensions. The HSFCM opens a new avenue for virus characterization.*

Viruses are by far the most abundant biological entities on our planet.[1] Whereas animal viruses are notoriously responsible for a large number of fatal diseases, plant viral pathogens cause significant losses in crop yields worldwide each year. On the other hand, the high transfection efficiency of viral gene-therapy vectors and their monodisperse structures with precise shapes and sizes make viral particles powerful drug-delivery vehicles and versatile nanotechnology building blocks.[2–4] Therefore, the high-resolution and high-throughput analysis of single viral particles is of great importance for virology research, disease diagnosis and treatment, and biotechnology and nanotechnology applications.

Transmission electron microscopy (TEM) has historically been the method of choice for determining the size and morphology of single viruses. However, the tedious processes required for sample preparation and image analysis, along with the high cost, prevent its use on a routine basis. Recently, many newly developed single-particle techniques have been applied to single-virus analysis, such as surface plasmon resonance imaging,[5] whispering-gallery-mode microcavities,[6] suspended micro- and nanochannel resonators,[7] scanning probe microscopy,[8] resistive pulse sensing with nanopores,[9] and nanoparticle tracking analysis (NTA).[10] Although some of these techniques have proven to be very useful in various fields, a simple and practical approach with exceptional sensitivity and high resolution remains to be developed. The real-time, label-free analysis of the size and composition of individual viral particles could be enabled by the quantification of their elastically scattered light intensity. However, the sixth-power dependence of the scattered light intensity on the particle size and the low dielectric contrast with the surrounding medium make it extremely challenging to discriminate single viruses over background scattering. Recently, Manoharan et al. reported the label-free tracking of individual cowpea chlorotic mottle viruses (28 nm in diameter) in a single-mode silica fiber with a subwavelength nanofluidic channel.[11] This is the smallest virus that has been detected at the single virion level using purely elastic scattering, yet sample clogging could be a severe problem. Although the scattered intensity scales with the sixth power, interferometric techniques can benefit from mixing with a reference beam and thus allow for third power dependence. The detection of bacteriophage lambda, empty capsids of simian virus 40 (45 nm in diameter), and even single proteins has been achieved.[12–14]

Flow cytometry is a high-throughput technique for single-cell analysis. Although great efforts have been made with regard to single virus detection,[15,16] it has been difficult to detect viruses smaller than 80 nm by label-free light scattering measurements. By adopting strategies for single-molecule fluorescence detection in a sheath flow,[17] we have recently developed a high sensitivity flow cytometry (HSFCM) method, which enables the real-time detection of the light scattering of single silica and gold nanoparticles with diameters as small as 24 nm and 7 nm, respectively.[18] Herein, we report a rapid high-resolution approach for virus characterization by applying the HSFCM to precisely quantify the ultraweak elastically scattered light from single viral particles.

The laboratory-built HSFCM is shown in Figure 1 a. The sample fluid was hydrodynamically focused to a very fine stream (ca. 1.4 μm) at the exit of a tapered capillary (40 μm inner diameter, 240 μm outer diameter) by the sheath flow. As the sample stream is located far from the windows of the cuvette (a 250 μm × 250 μm square-bore quartz flow channel) and is surrounded by a sheath flow of pure water, the

[*] L. Ma,[+] Dr. S. Zhu,[+] Y. Tian, W. Zhang, S. Wang, C. Chen, Dr. L. Wu, Prof. Dr. X. Yan
Collaborative Innovation Center of Chemistry for Energy Material
The MOE Key Laboratory of Spectrochemical Analysis & Instrumentation
The Key Laboratory for Chemical Biology of Fujian Province
Department of Chemical Biology
College of Chemistry and Chemical Engineering
Xiamen University
Xiamen 361005 (P.R. China)
E-mail: xmyan@xmu.edu.cn
Homepage: http://xmyan.xmu.edu.cn

[+] These authors contributed equally to this work.

Supporting information for this article can be found under: http://dx.doi.org/10.1002/anie.201603007.

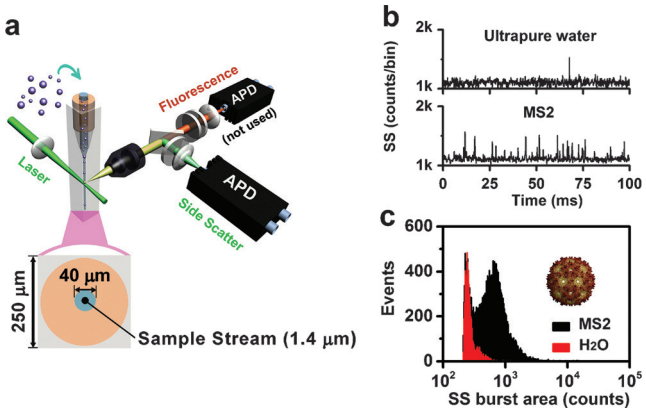

Figure 1. a) The laboratory-built HSFCM for the light-scattering detection of single viruses with the sheath flow system and the cross-section (not to scale) of the capillary and fluid streams. b) Representative SS burst traces of ultrapure water and the bacteriophage MS2. c) SS burst-area distribution histograms of ultrapure water and the bacteriophage MS2. Each distribution histogram was derived from data collected over 1 min. Laser excitation power: 200 mW; focused laser spot: 6.4 μm diameter.

background scattering from the cuvette windows can be efficiently blocked by simple spatial masking. Here, the small active area of the avalanche photodiode (APD) detector (ca. 180 μm in diameter) acts as a limiting aperture to prevent the light scattered outside the probed volume from reaching the detector. Bacteriophage MS2, an icosahedral, positive-sense, single-stranded RNA virus with a diameter of approximately 27 nm,[19] was used to assess the sensitivity of the method for single-virus detection. As elastic light scattering is a spontaneous process, a higher excitation energy density was used to enhance the intensity of the scattered photons. The excitation beam from a 200 mW, 532 nm continuous-wave laser was focused to a spot with a diameter of approximately 6.4 μm ($1/e^2$), which resulted in an excitation energy density of $6.2\times10^5\ W\,cm^{-2}$. Figure 1b shows the representative side scatter (SS) burst traces for ultrapure water filtered through a 0.22 μm filter and the MS2 viruses; in both traces, a continuous background signal of about 1100 counts/bin was observed (for a bin width of 100 μs). The signal to noise (S/N) ratio, which was calculated as the average burst height of all of the nanoparticles detected in 1 min divided by the standard deviation of the background signal (noise), was 11 for the MS2 viruses, indicating that the HSFCM provides exceptional sensitivity in discerning MS2 viruses against the background noise.

Based on the theory of Rayleigh scattering, the scattering cross-section of a nanoparticle is not only determined by the particle size but also influenced by the refractive index contrast, which is the ratio of the refractive indexes of the particle and the medium.[20] A silica nanoparticle (with a refractive index of 1.46) scatters 3.8 fold less light than a polystyrene nanoparticle (with a refractive index of 1.59) of the same size at a wavelength of 532 nm. The exact refractive index of the virus is not known, but it can be assumed to be 1.45 or 1.46, which is similar to that of proteins[21] and DNA.[22] The effect of the refractive index on the light-scattering detection of single viruses was examined with the bacteriophage T7, a bacterial virus with an icosahedral capsid head with a diameter of about 60 nm,[23] along with silica nanospheres and polystyrene nanobeads of a comparable size.

To avoid signal saturation and to ensure a more uniform illumination of the sample stream, the laser excitation power was attenuated to 16 mW, and the laser beam was focused to a spot with a diameter of 16 μm ($1/e^2$), which resulted in a reduced background count of about 200 counts/bin. Representative SS burst traces for bacteriophage T7 virions, 60 nm silica nanospheres, and 63 nm polystyrene nanobeads are shown in Figure 2a, and the measured S/N ratios were 94, 97, and 635, respectively. Compared with the highly monodisperse silica nanospheres of 60 ± 2 nm diameter (see the Supporting Information, Figure S1), the naturally occurring bacteriophage T7 is more uniform with a very narrow distribution profile for the light-scattering intensity. Considering the sixth-power dependence of the scattering intensity on the particle size, the 12% coefficient of variation (CV, the ratio of the standard deviation and the mean) of the scattering intensity for the T7 virion corresponds to a 1.9% variation in the size measurements, which can be ascribed to the actual particle size distribution and the measurement uncertainty. The comparable burst height/burst area for the T7 virions and

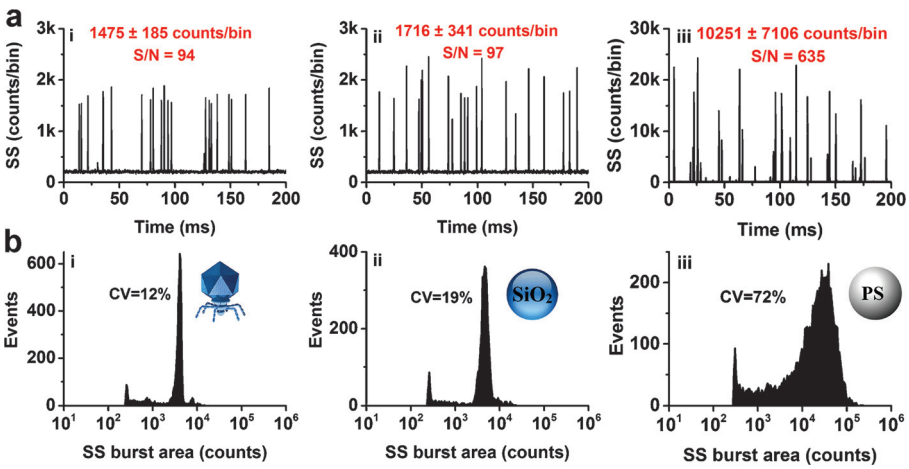

Figure 2. HSFCM analysis of single nanoparticles by light-scattering detection. a) Representative SS burst traces of the bacteriophage T7 virions (i), 60 nm diameter silica nanospheres (ii), and 63 nm diameter polystyrene nanobeads (iii). b) SS burst-area distribution histograms of the bacteriophage T7 virions (i), 60 nm diameter silica nanospheres (ii), and 63 nm diameter polystyrene nanobeads (iii). The nanoparticle concentrations were $2–5\times10^9\ mL^{-1}$. Laser excitation power: 16 mW; focused laser spot: 16 μm diameter.

60 nm silica nanospheres confirms that the virus and silica nanoparticles exhibit comparable refractive indices.[5] The approximately 6-fold higher scattering intensity observed for the polystyrene nanobeads of 63 nm diameter compared to that of the 60 nm silica nanospheres agrees with the theoretical prediction of a 5.1-fold increase.

The applicability of the HSFCM for the discrimination and size determination of viruses in a mixture was examined by using bacteriophages as the model system because bacteriophages are the most abundant viruses, are safe to handle, and have been instrumental to the study of the basic principles of virology. One bacteriophage from each of the four most extensively studied phage families, *Inoviridae*, *Podoviridae*, *Siphoviridae*, and *Myoviridae*, was selected, and they were mixed. The structural dimensions of the M13, T7, λ, and PP01 phages are listed in Table 1. PP01 is a T2-type phage that infects the *E. coli* O157:H7 strain with high specificity.[24] A representative SS burst trace is shown in Figure 3a. The SS burst-area distribution histogram indicates that these four types of viruses can be resolved with baseline separation (Figure 3b) even though the size difference between bacteriophages T7 and λ, for example, is only 4 nm. Interestingly, the profile of PP01 is bimodal, a feature that can be ascribed to the retraction or extension of the tail fibers[25] as was confirmed by TEM measurements (Figure S2).

To measure the actual size of single viruses from their scattering intensities, a standard calibration curve was constructed with monodisperse silica nanospheres of five different diameters ranging from 43 to 113 nm. When the centroids of the SS burst areas obtained from the fitted Gaussian curves for each nanosphere population (Figure 3c) were plotted as a function of the diameters determined by TEM (Figure S3), a 5.95th order dependence of the scattering intensity on the particle size was determined, in excellent agreement with Rayleigh scattering theory (Figure 3d). Using this calibration curve, the SS burst area of every single virus was converted into the corresponding particle size (Figure 3e). The measured particle sizes were 41.8, 60.6, 74.4, and 99.6 nm for the M13, T7, λ, and PP01 bacteriophages, respectively. Virus samples containing each of these four different types of viruses were also analyzed in parallel by dynamic light scattering (DLS), and the compiled size distribution profiles are shown in Figure 3f. For the mixture of these four different types of viruses, only one peak was observed (black dashed/dotted line in Figure 3f).

Table 1 lists the diameters for these four types of viruses measured by HSFCM and DLS, along with the equivalent particle diameters (EPDs). Compared with the hydrodynamic diameters determined by DLS, the optical diameters measured by HSFCM are in better agreement with the EPDs. The slight deviation for bacteriophage λ could be attributed to an orientation effect induced by its long rigid tail as the virus transits through the polarized laser beam. From the perspective of measurement precision, HSFCM performs better than DLS. For example, the standard deviation of the measured particle sizes was 1.3 nm for bacteriophages T7 whereas that of the values obtained by DLS was approximately 10-fold higher. These

Table 1: Comparison of the accuracy and precision of the HSFCM, DLS, and TEM techniques in virus size measurements.

Virus	Family	Capsid [nm]	Tail [nm]	EPD [nm][a]	HSFCM [nm]	DLS [nm]
M13	*Inoviridae*	ca. 6.5×930[b]	–	38.9	41.8±3.2	49.0±16.9
T7	*Podoviridae*	60[c]	17×8	60.2	60.6±1.3	57.4±13.3
λ	*Siphoviridae*	63[d]	150×8	64.2	74.4±1.4	65.1±15.0
PP01	*Myoviridae*	85×110[e]	110×25	96.5	99.6±4.5	110.5±29.0

[a] EPD: The equivalent particle diameter is defined as the diameter of a sphere with a volume equivalent to the volume of a virus obtained by approximating its shape to a cylinder (M13), a sphere on top of a cylinder (T7, λ), or a spheroid on top of a cylinder (PP01). See the Supporting information for details. [b] Ref. [26]. [c] Ref. [23]. [d] Ref. [27]. [e] Ref. [23].

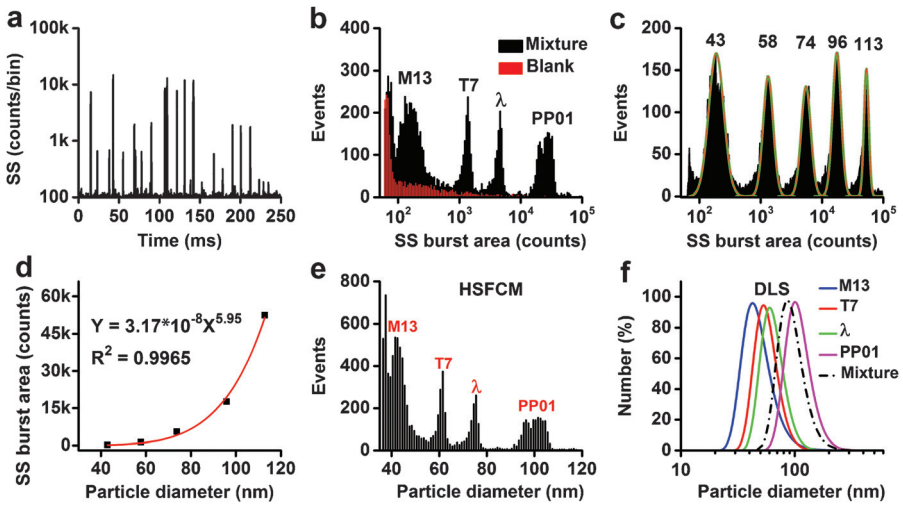

Figure 3. Differentiation and size measurement of different virus types in a mixture by the HSFCM approach. a) Representative burst traces of a mixture of the bacteriophages M13, T7, λ, and PP01. b) SS burst-area distribution histograms of ultrapure water (blank) and the virus mixture, derived from data collected over 1 min. c) SS burst-area distribution histogram of a mixture of silica nanoparticles of five different diameters ranging from 43 to 113 nm, and the fit of the data to a sum of Gaussian peaks. d) Plot of the Gaussian fitted SS burst areas as a function of the particle sizes determined by TEM. e) Particle size distribution histogram with a bin width of 0.5 nm for the mixture of four different types of bacteriophages obtained by HSFCM. f) Normalized virus size distribution histograms (by particle number) for the four types of virus samples measured separately and for the mixture (the black dashed/dotted line) by DLS. The laser power was attenuated to 10 mW to avoid APD saturation.

results demonstrate that by using silica nanoparticles as the calibration standards, HSFCM enables accurate virus size measurements with a resolution comparable to that of TEM. Particularly, with a throughput of up to 10000 particles per minute, a statistically reliable size distribution profile can be obtained in 2–3 min.

Purity assessment of virus products is indispensable in many biotechnology applications. As we can see from Figure 4a, many particles can coexist in the lysates of host cells infected with a wild-type phage, including cell debris, DNA-free proheads, empty capsids (after DNA ejection), and mature virions. Figure 4bi and ii show the SS burst-area distribution histograms of a crude extract of bacteriophage T7 obtained by polyethylene glycol precipitation and of the purified products after density gradient centrifugation, respectively. For the crude extract, the peak of lower scattering intensity is assumed to consist of cell debris, proheads, and empty capsids, whereas the peak of higher intensity can be ascribed to the mature virions. In our HSFCM setup, the hydrodynamically focused sample stream (ca. 1.4 μm) was completely illuminated within the central region of the interrogating laser beam (16 μm), and nearly 100% detection efficiency can be achieved.[28] Therefore, single particle enumeration can be used to quantify the abundance of each population, and the percentage of mature virions detected improved from 29.5% in the crude extract to 93.6% after purification.

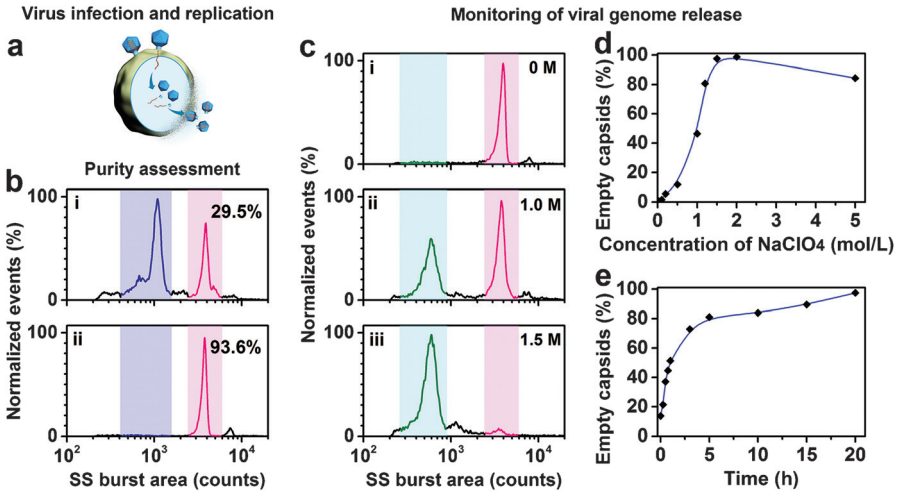

Figure 4. Purity assessment and genome release study of viruses by HSFCM. a) Schematic representation of the virus infection and replication process of bacteriophage T7. b) Purity assessment of the virus products. Normalized SS burst-area distribution histograms of the crude extract of the bacteriophage T7 (i) and the purified products upon density gradient centrifugation (ii). c) Analysis of the $NaClO_4$ triggered DNA ejection process of the bacteriophage T7. Normalized SS burst-area distribution histograms of the bacteriophage T7 after 20 h of $NaClO_4$ treatment at concentrations of 0 M, 1.0 M, and 1.5 M (i–iii, respectively). The signals that correspond to the mature virions are highlighted in pink, and those corresponding to the proheads and capsids are shown in purple and cyan, respectively. d) Effect of the $NaClO_4$ concentration on the generation of empty T7 capsids. e) Dynamic monitoring of the viral genome release process upon treatment with 1.5 M $NaClO_4$ solution.

The HSFCM method was further applied to monitor the viral genome release process. Figure 4cii indicates that after 20 h treatment with 1.0 M $NaClO_4$ solution, in addition to the mature virions, a peak with a lower scattering intensity appeared, which can be ascribed to the empty capsid of bacteriophage T7. The population of empty capsids reached 95% when a 1.5 M solution of $NaClO_4$ was used. These results confirm that simply by detecting the scattering signal of individual particles, HSFCM can easily distinguish the empty capsid of T7 from mature T7 virions. The effect of the $NaClO_4$ concentration on the production of the T7 capsid is shown in Figure 4d. To further probe the capsid–genome interplay, the dynamic process of DNA release was monitored (Figure 4e). It has been reported that DNA ejection from phages is a spontaneous process in vitro, but neither the kinetics nor the thermodynamics are fully understood.[29] It is interesting to note that as soon as $NaClO_4$ was added (ca. 1 min from sample injection to analysis), approximately 13% of the virions completed the ejection of their viral genome, and this percentage increased to 21% after 15 min. The action rate of DNA release increased during the first 5 h and decreased afterwards. After 20 h, approximately 97% of the virions had completed the release of their viral genome. It is worth noting that the scattering signals of the proheads in the crude extract of T7 (Figure 4bi, peak value of about 1100 counts) are slightly higher than those of the empty capsids generated by DNA release from the mature virions (Figure 4ciii, peak value of ca. 600 counts).

In summary, the HSFCM method provides a simple and practical approach for the high-resolution and high-throughput characterization of viruses. The exceptional sensitivity of the HSFCM enables us to detect viruses with diameters of less than 30 nm and efficiently resolve different types of viruses in a mixture. Broad applications in the analysis of virus products during both the manufacturing process and storage can be envisioned. The capability of the HSFCM in discriminating the subtle structural differences of the same viral particles, that is, the differentiation of bacteriophages PP01 with retracted or extended tail fibers, the complete separation of the empty capsids from the mature virions of T7 bacteriophages, and the differentiation of capsids before DNA packaging (proheads) and after DNA release (empty capsids), indicates that the HSFCM method could be an efficient approach for virology studies. Yet, it is worth noting that with the presence of a large number of scattering objects, such as in the case of virus detection in serum or plasma, nucleic acid

fluorescence staining is needed to differentiate single viruses. Thus the fluorescence channel of the HSFCM setup can be applied to further extend the analysis of viruses under many realistic conditions.

Acknowledgements

We acknowledge support from the National Natural Science Foundation of China (21225523, 91313302, 21027010, 21475112, and 21521004), the National Key Basic Research Program of China (2013CB933703), and the Program for Changjiang Scholars and Innovative Research Team in University (IRT13036).

Keywords: analytical methods · bacteriophages · flow cytometry · light-scattering detection · viruses

How to cite: *Angew. Chem. Int. Ed.* **2016**, *55*, 10239–10243
Angew. Chem. **2016**, *128*, 10395–10399

[1] C. A. Suttle, *Nat. Rev. Microbiol.* **2007**, *5*, 801–812.
[2] N. F. Steinmetz, *Nanomedicine* **2010**, *6*, 634–641.
[3] P. C. Jordan, D. P. Patterson, K. N. Saboda, E. J. Edwards, H. M. Miettinen, G. Basu, M. C. Thielges, T. Douglas, *Nat. Chem.* **2016**, *8*, 179–185.
[4] Z. Liu, J. Qiao, Z. W. Niu, Q. Wang, *Chem. Soc. Rev.* **2012**, *41*, 6178–6194.
[5] S. Wang, X. Shan, U. Patel, X. Huang, J. Lu, J. Li, N. Tao, *Proc. Natl. Acad. Sci. USA* **2010**, *107*, 16028–16032.
[6] L. He, S. K. Özdemir, J. Zhu, W. Kim, L. Yang, *Nat. Nanotechnol.* **2011**, *6*, 428–432.
[7] S. Olcum, N. Cermak, S. C. Wasserman, K. S. Christine, H. Atsumi, K. R. Payer, W. J. Shen, J. C. Lee, A. M. Belcher, S. N. Bhatia, S. R. Manalis, *Proc. Natl. Acad. Sci. USA* **2014**, *111*, 1310–1315.
[8] L. Fumagalli, D. Esteban-Ferrer, A. Cuervo, J. L. Carrascosa, G. Gomila, *Nat. Mater.* **2012**, *11*, 808–816.
[9] J. L. Fraikin, T. Teesalu, C. M. McKenney, E. Ruoslahti, A. N. Cleland, *Nat. Nanotechnol.* **2011**, *6*, 308–313.
[10] P. Kramberger, M. Ciringer, A. Strancar, M. Peterka, *Virol. J.* **2012**, *9*, 265.
[11] S. Faez, Y. Lahini, S. Weidlich, R. F. Garmann, K. Wondraczek, M. Zeisberger, M. A. Schmidt, M. Orrit, V. N. Manoharan, *ACS Nano* **2015**, *9*, 12349–12357.
[12] P. Kukura, H. Ewers, C. Müller, A. Renn, A. Helenius, V. Sandoghdar, *Nat. Methods* **2009**, *6*, 923–927.
[13] A. Mitra, F. Ignatovich, L. Novotny, *Biosens. Bioelectron.* **2012**, *31*, 499–504.
[14] M. Piliarik, V. Sandoghdar, *Nat. Commun.* **2014**, *5*, 4495.
[15] M. Hercher, W. Mueller, H. M. Shapiro, *J. Histochem. Cytochem.* **1979**, *27*, 350–352.
[16] H. B. Steen, *Cytometry Part A* **2004**, *57*, 94–99.
[17] W. P. Ambrose, P. M. Goodwin, J. H. Jett, A. Van Orden, J. H. Werner, R. A. Keller, *Chem. Rev.* **1999**, *99*, 2929–2956.
[18] S. Zhu, L. Ma, S. Wang, C. Chen, W. Zhang, L. Yang, W. Hang, J. P. Nolan, L. Wu, X. Yan, *ACS Nano* **2014**, *8*, 10998–11006.
[19] D. A. Kuzmanovic, I. Elashvili, C. Wick, C. O'Connell, S. Krueger, *Radiat. Phys. Chem.* **2006**, *75*, 359–368.
[20] C. F. Bohren, D. R. Huffman, *Absorption and scattering of light by small particles*, Wiley, New York, **1983**.
[21] S. Busse, V. Scheumann, B. Menges, S. Mittler, *Biosens. Bioelectron.* **2002**, *17*, 704–710.
[22] L. Moiseev, M. S. Unlu, A. K. Swan, B. B. Goldberg, C. R. Cantor, *Proc. Natl. Acad. Sci. USA* **2006**, *103*, 2623–2628.
[23] F. A. Murphy, C. M. Fauquet, D. H. Bishop, S. A. Ghabrial, A. W. Jarvis, G. P. Martelli, M. A. Mayo, M. D. Summers, *Virus taxonomy: classification and nomenclature of viruses. Sixth report of the International Committee on Taxonomy of Viruses*, Springer, New York, **1995**.
[24] M. Morita, Y. Tanji, K. Mizoguchi, T. Akitsu, N. Kijima, H. Unno, *FEMS Microbiol. Lett.* **2002**, *211*, 77–83.
[25] C. Gordon, *J. Mol. Biol.* **1972**, *65*, 435–445.
[26] J. W. Kehoe, B. K. Kay, *Chem. Rev.* **2005**, *105*, 4056–4072.
[27] S. R. Casjens, R. W. Hendrix in *Encyclopedia of life sciences*, Wiley, Chichester, **2001**.
[28] S. Zhu, L. Yang, Y. Long, M. Gao, T. Huang, W. Hang, X. Yan, *J. Am. Chem. Soc.* **2010**, *132*, 12176–12178.
[29] I. J. Molineux, D. Panja, *Nat. Rev. Microbiol.* **2013**, *11*, 194–204.

Received: March 30, 2016
Revised: May 18, 2016
Published online: July 26, 2016

